Proceedings of the ASME 2022
International Design Engineering Technical Conferences and
Computers and Information in Engineering Conference
IDETC-CIE2022
August 14-17, 2022, St. Louis, Missouri

DETC2022-89825

# A NOVEL VARIABLE STIFFNESS COMPLIANT ROBOTIC LINK BASED ON DISCRETE VARIABLE STIFFNESS UNITS FOR SAFE HUMAN-ROBOT INTERACTION

Jiaming Fu<sup>1</sup>, Han Lin<sup>1</sup>, Wei Xu<sup>1</sup>, Dongming Gan<sup>1\*</sup>

<sup>1</sup>Polytechnic Institute, Purdue University, West Lafayette, IN47907, US

#### **ABSTRACT**

Variable stiffness manipulators balance the trade-off between manipulation performance needing high stiffness and safe human-robot interaction desiring low stiffness. Variable stiffness compliant links provide a solution to enable this flexible manipulation function in human-robot co-working scenarios. In this paper, we propose a novel variable stiffness link based on discrete variable stiffness units (DSUs). A DSU is a parallel guided beam that can adjust stiffness discretely by changing the cross-sectional area properties of the hollow beam segments. The variable stiffness link (named Tri-DSU) consists of three tandem DSUs to achieve eight stiffness modes and a maximum stiffness change ratio of 31. To optimize the design, stiffness analysis of the DSU and Tri-DSU under various configurations and forces was performed by a derived theoretical model compared with finite element analysis (FEA). The analytical stiffness model is derived using the approach of serially connected beams and superposition combinations. It works not only for thin-walled flexure beams but also for general thick beam models. 3-D printed prototypes were built to verify the feature and performance of the Tri-DSU in comparison with the FEA and analytical model results. It's demonstrated that our analytical model can accurately predict the stiffnesses of the DSU and Tri-DSU within a certain range of parameters. The developed variable stiffness link method and analytical model are extendable to multiple DSUs with different sizes and parameter configurations to achieve modularization and customization. The advantages of the stiffness change mechanism are rapid actuation, simple structure, and compact layout. These methods and results provide a new conceptual and theoretical basis for the development of new reconfigurable cobot manipulators, variable stiffness structures, and compliant mechanisms.

\* Please address all correspondence to this author, dgan@purdue.edu

Keywords: variable stiffness link, discrete variable stiffness, parallel beam, stiffness modeling, compliant mechanism

## 1. INTRODUCTION

Due to technical reasons, humans are excluded from the work area to ensure safety during traditional industrial robots working [1]. For example, the welding process in the automobile manufacturing process does not require human participation at all, and safety fences are used to separate workers and robots [2]. However, many jobs require human participation that cannot be automated to a high degree by robots so far [3]. As a result, a collaborative robot (cobot), a type of robot that can safely interact directly with humans, is growing at a rapid pace [4]. In manufacturing, the introduction of collaborative robots can make full use of the efficiency of robots to compensate for the low human precision, strength, and durability, while retaining human intelligence and skills [5].

Researchers have explored from the perspective of materials, using soft materials to make robotic arms to reduce impact forces during collisions. In [6], the arm was wrapped with pneumatic artificial muscles and inflatable sleeves. In [7], a soft robotic arm driven by shape memory alloy (SMA) coils was reported. In [8], a soft robotic arm (SRA) made from nylon fabric was proposed. However, while low stiffness brings safe interaction, it compromises performance on accuracy and payload which needs high stiffness. This has led to variable stiffness manipulators to balance the two sides.

To enable variable compliant manipulation, researchers innovate from the perspective of mechanical design by adding variable stiffness actuators (VSA) to the robot joints to achieve safe interaction. Some VSAs are based on the variable impedance actuation (VIA) method to increase the torque

bandwidth and reduce structure sizes [9–12]. In [13,14], the VSAs could adjust stiffness by changing the effective beam length to achieve continuous variable stiffness. In [15,16], the VSAs can achieve discrete variable stiffness.

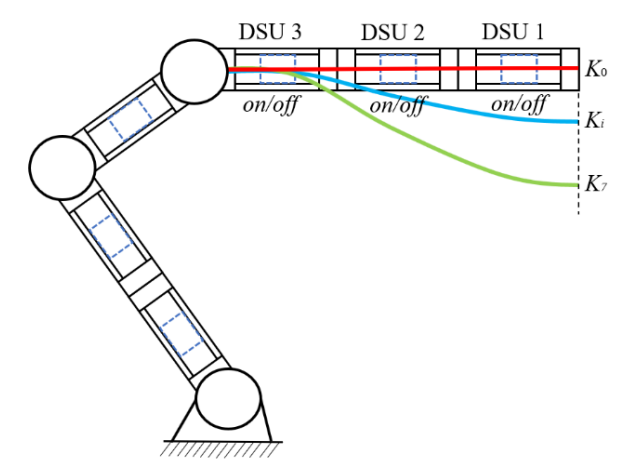


FIGURE 1: COBOT WITH VARIABLE STIFFNESS LINKS

Another method in developing variable stiffness compliant manipulators is to design a variable stiffness link. However, compared to VSAs and compliant grippers [17,18], little research has been done on compliant robotic links. A variable stiffness robotic arm [19,20] based on a rotating beam link was proved to be feasible. A variable stiffness robotic arm [21,22] based on compliant parallel guide beams has also been validated.

The majority of published variable stiffness robotic links are continuous variable stiffness, but there are many cases where continuous adjustment is not necessary. Inspired by our previous work on discrete variable stiffness actuators [23,24], the design of a compact discrete variable stiffness robot link with fast stiffness change and a large stiffness change ratio provides a more practical development direction. We improved the reconfigurable variable-stiffness parallel beam (VSPB) [25] and developed a discrete variable stiffness unit (DSU), which achieves discrete variable stiffness by changing the crosssectional area property. The main structure of the DSU is a parallel guided beam that can adjust stiffness by a push-pull solid block to the cavity of the beam. The solid block is mounted on the stroke of a linear actuator, which is fixed to the side of the solid body of the DSU near the pedestal end of the robotic arm. The variable stiffness robotic link (Tri-DSU) consists of three tandem DSUs, each of which can be adjusted individually to achieve eight stiffness modes, as shown in Fig.1.

Compared with existing compliant links, the Tri-DSU has the following main advantages: (1) It has a simple and compact structure and does not need motors. (2) It has low energy consumption because the linear actuator module operates on very low power and is energized only when the system is switching stiffness modes. (3) It provides fast stiffness change as the linear actuator module is activated in an on/off manner to complete the variable stiffness task, which improves the efficiency of the system. We also derive accurate analytical models for DSU and Tri-DSU, which do not require

experimental determination of coefficients each time the model parameters are changed compared to the pseudo-rigid body (PRB) model [26,27].

The paper is organized as follows: Section 2 introduces the mechanical design and concept implemented for the stiffness variation of Tri-DSU; Section 3 develops the analytical model of the stiffness variation. Section 4 compares the analytical model, FEA, and experimental values; Section 5 concludes the work.

## 2. CONCEPT OF THE DESIGN

## 2.1 Working principle of stiffness variation

As shown in Fig. 2, the Tri-DSU is a variable stiffness link consisting of three serial-connected DSUs. The main structure of the DSU is a parallel guided beam that can adjust stiffness by a push-pull solid block to the cavity of the beam. The on/off mode of the block changes the second area of the moment of inertia of the beam leading to stiffness varying. The illustrated DSU design is 3-D printed with PLA with dimensions  $100 \times 20 \times 20$  mm. The length of the cavity is 80 mm, and the thickness of the parallel beams is 1 mm. A linear actuator is fixed to the solid segment on the side of the DSU near the pedestal end of the arm to reduce the impact on the flexible structure of the DSU because the solid segment has almost no deformation. The model of the linear actuator is ACTUONIX PQ12-P which has a compact size, but its stroke length is 20 mm. The solid block is mounted on the stroke of the linear actuator, and the stroke passes through the cavity near the solid segment. When the parallel beam bends, the deformation of the middle part of the beam is large and the deformation of the ends is small. Therefore, the stroke does not touch the beam and does not interfere with the deformation of the beam. When the stroke is extruded, the solid block is pushed out of the cavity of the parallel beam, called off mode, now the DSU has relatively low stiffness and high compliance. When the stroke is retracted, the solid block is pulled into the cavity, called on mode, where the DSU has relatively high stiffness and accuracy. The extrusion or retraction process of the stroke takes only 0.2 s, which means that the DSU can change its stiffness rapidly. When the beam has a large deformation, the block cannot be inserted or pushed out smoothly, so the DSU can only achieve offline variable stiffness, which still covers most of the application scenarios.

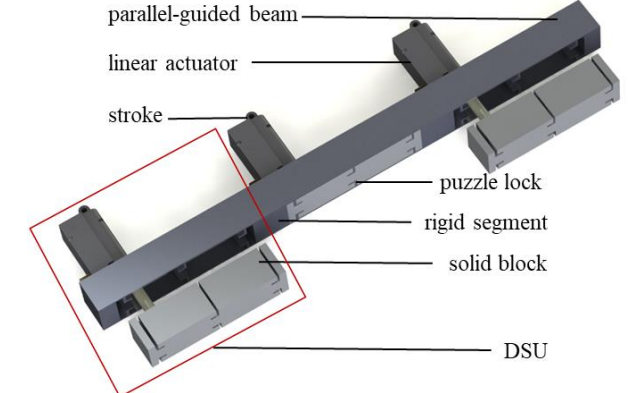


FIGURE 2: THE STIFFNESS CHANGE PRINCIPLE OF TRI-DSU

The Tri-DSU consists of three DSUs connected in series, so each DSU can be adjusted individually to achieve the eight stiffness modes of the entire system. When all DSUs are in off mode, the Tri-DSU is in off-off-off (FFF) mode, and the system has the lowest stiffness. When two DSUs are in off mode and another DSU is in on mode, the Tri-DSU may be in off-off-on (FFN) mode, off-on-off (FNF) mode, or on-off-off (NFF) mode. In these three cases, the stiffness of the Tri-DSU is relatively low and close to each other, only the position of the flexible segment is different. When two DSUs are in on mode and the other two DSUs are in off mode, the Tri-DSU may be in on-on-off (NNF) mode, on-off-on (NFN) mode, or off-on-on (FNN) mode. In these three cases, the stiffness of Tri-DSUs is relatively high. When all DSUs are in on mode, the Tri-DSU is in on-on-on (NNN) mode, the system has the highest stiffness. Theoretically, the Tri-DSU in such a parameter configuration can achieve 57 times the variation in stiffness.

The design of the DSU can be modular and customizable. The dimensions and materials of the prototypes are only examples and can be adapted to actual requirements, or more DSUs can be connected in series to construct multiple DSUs structures. In a DSU, the hollow parallel beam part in the middle and the solid rigid parts at both ends also have a certain thickness rather than treated as thin walls [28,29]. In order to systematically elaborate the variable stiffness principle of DSUs, a generalized stiffness modeling approach is developed to lay the theoretical foundation for further design and application of this new variable stiffness mechanism.

## 3. STIFFNESS MODELING

# 3.1 Analytical stiffness model of the DSU

Fig. 3 illustrates the basic geometry structure of a DSU. The total length of the parallel guided beam with a block inside is L in an x-y coordinate system: the x-axis direction is horizontal along the long axis of the beam to the right and the y-axis is perpendicular to the x-axis and downward while the z-axis is ignored since the beam is considered only working on the x-y plane.

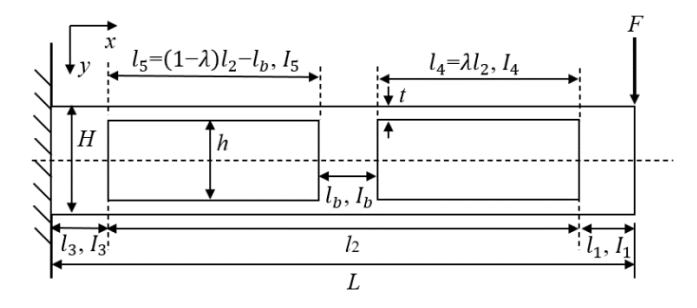


FIGURE 3: FREE BODY DIAGRAM OF a DSU

Assuming that the left end of the beam is fixed to the wall, and downward force F acts perpendicular to the x-axis and is applied to the right end of the beam. In this model, parasitic error motions[30] in the x-axis direction that are undesired motions in the degree of constraint will be ignored, because their value is

too small compared with the deflection in the *y*-direction. Obviously, most deflection of the beam will be generated by the compliant segments, which are  $l_4$  and  $l_5$ , but solid segments of  $l_1$ ,  $l_b$ , and  $l_3$  should not be ignored because they have a certain thickness in real applications and their elasticity will affect the accuracy of the model. The stiffness of the DSU is adjustable by the block in the cavity. When the DSU is in the off mode,  $l_b$  is equal to zero, and if the DSU is switched to on mode,  $l_b$  will be greater than zero.

The beam is divided into five segments in this case, where  $l_1$ ,  $l_b$ , and  $l_3$  are solid bodies with the moment of inertia  $I_1$ ,  $I_b$ , and  $I_3$  respectively. The segments  $l_4$  and  $l_5$  are parallel-beam mechanisms with the moment of inertia  $I_4$  and  $I_5$ . The length of  $l_2$  is equal to the sum of  $l_4$ ,  $l_b$ , and  $l_5$ . To facilitate calculation and analysis, we can parameterize  $l_4$  and make it  $\lambda l_2$ , then  $l_5$  is equal to  $(1-\lambda)$   $l_2-l_b$ . To get an accurate result, we compute the deflections of the beam segment-by-segment and then superpose the results together. The calculation process of the deflection and stiffness of the DSU is shown below.

The height of the DSU is H, and the height of the cavity is h. Thus, the thickness of the leaf springs in  $l_4$  and  $l_5$  are t = (H - h)/2. The width b of the beam is not marked in Fig. 3, which is perpendicular to the surface of the paper. Then the moment of inertia of each segment can be obtained:

$$I_1 = I_3 = I_b = \frac{H^3 b}{12} \tag{1}$$

$$I_4 = I_5 = \frac{t^3 b}{12} \tag{2}$$

First, segments  $l_2$  and  $l_3$  are considered rigid, and only segment  $l_1$  is compliant. Thus, the deflection  $\delta_1$  at the end of  $l_1$  can be calculated by the normal cantilever beam equation, where E is Young's modulus of the DSU.

$$\delta_1 = \frac{Fl_1^3}{3EI_1} \tag{3}$$

Next, the other parts are treated as rigid bodies and only segment  $l_4$  is compliant. In addition to the forces that cause a deflection angle and deflection to  $l_4$ , the bending moment from  $l_1$  also causes a deflection angle and deflection to L. Based on the theory of parallel guided mechanism [31], then the following are derived formulas to calculate the total deflection angle  $\theta_2$  and total deflection  $\delta_2$  of the compliant segment  $l_4$  under both force and moment:

$$\theta_2 = \frac{t^2}{6h^2} \left( \frac{Fl_1(\lambda l_2)}{El_4} + \frac{F(\lambda l_2)^2}{2El_4} \right) \tag{4}$$

$$\delta_2 = \frac{F(\lambda l_2)^3}{24El_4} + \frac{t^2}{12h^2} \left( \frac{Fl_1(\lambda l_2)^2}{El_4} + \frac{F(\lambda l_2)^3}{2El_4} \right) \tag{5}$$

Similarly, the other segments are treated as rigid bodies to calculate the deflection angle  $\theta_3$  and deflection  $\delta_3$  of segment  $l_b$ .

$$\theta_3 = \frac{Fl_b^2}{2EI_b} + \frac{F(l_1 + \lambda l_2)l_b}{EI_b}$$
 (6)

$$\delta_3 = \frac{Fl_b^3}{3El_b} + \frac{F(l_1 + \lambda l_2)l_b^2}{2El_b} \tag{7}$$

The deflection angle  $\theta_4$  and deflection  $\delta_4$  of the compliant segment  $l_5$  are:

$$\theta_4 = \frac{t^2}{6h^2} \left( \frac{F(l_1 + \lambda l_2 + l_b)[(1 - \lambda)l_2 - l_b]}{EI_5} + \frac{F[(1 - \lambda)l_2 - l_b]^2}{2EI_5} \right)$$
(8)

$$\delta_4 = \frac{F[(1-\lambda)l_2 - l_b]^3}{24El_5} + \frac{t^2}{12h^2} \left( \frac{\frac{F(l_1 + \lambda l_2 + l_b)[(1-\lambda)l_2 - l_b]^2}{El_5}}{+\frac{F[(1-\lambda)l_2 - l_b]^3}{2El_5}} \right)$$
(9)

To compute the deflection angle  $\theta_5$  and deflection  $\delta_5$  of segment  $l_3$  as below:

$$\theta_5 = \frac{Fl_3^2}{2EI_3} + \frac{F(l_1 + l_2)l_3}{EI_3} \tag{10}$$

$$\delta_5 = \frac{Fl_3^3}{3EI_3} + \frac{F(l_1 + l_2)l_3^2}{2EI_3} \tag{11}$$

Finally, all the deflection acting on the end of the DSU are accumulated to get its maximum deflection  $\delta_A$  and the stiffness  $k_A$  can be calculated using Eq. (12-13).

$$\delta_A = \delta_1 + \delta_2 + \delta_3 + \delta_4 + \delta_5 + \theta_2 l_1 + \theta_3 (l_1 + \lambda l_2) + \theta_4 (l_1 + \lambda l_2 + l_b) + \theta_5 (l_1 + l_2)$$
(12)

$$k_A = \frac{F}{\delta_A} \tag{13}$$

## 3.2 Analytical stiffness model of the Tri-DSU

As shown in Fig. 4, the Tri-DSU consists of three DSUs connected in series. To achieve modularity and customization, we develop a set of stiffness analytical models for Tri-DSU that is also adapted to multi-DSU. This model is based on the model in Section 3.1 for DSU with the same force conditions and coordinate system.

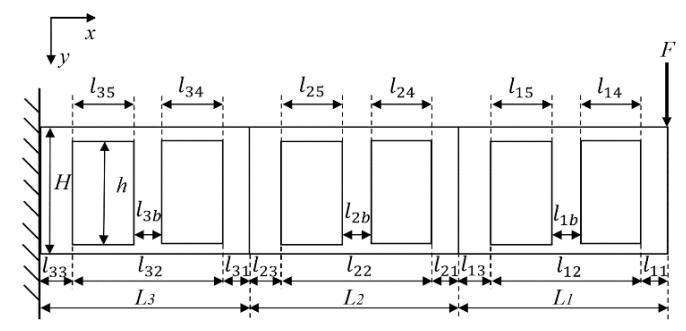


FIGURE 4: FREE BODY DIAGRAM OF TRI-DSU

In the case of Tri-DSU,  $l_{ij}$  represents the j-th segment in the i-th DSU from the free end to the fixed end. Therefore, the Tri-DSU is divided into 15 segments, from  $l_{11}$  to  $l_{33}$ . The  $l_{ij}$  represents the moment of inertia:

$$I_{i1} = I_{i3} = I_{ib} = \frac{H^3 b}{12} \tag{14}$$

$$I_{i4} = I_{i5} = \frac{t^3 b}{12} \tag{15}$$

To simplify the calculation, we constructed the following functions for the deflection angle and deflection of each segment changing under the action of forces and bending moments.  $\theta_{02}$  represents the total deflection angle of the compliant segments,  $l_{i4}$  and  $l_{i5}$ .  $\delta_{02}$  represents the total deflection of  $l_{i4}$  and  $l_{i5}$ .  $\theta_{03}$  and  $\delta_{03}$  represent the total angle and deflection of the solid segments,  $l_{i1}$ ,  $l_{ib}$ , and  $l_{i3}$ , except  $l_{11}$ .

$$\theta_{02}(F, l_{01}, l_{04}, I_{04}, t, h, E) = \frac{t^2 F}{6h^2} \left( \frac{l_{01} l_{04}}{E I_{04}} + \frac{l_{04}^2}{2E I_{04}} \right)$$
(16)

$$\delta_{02}(F, l_{04}, l_{012}, I_{04}, t, h, E) = \frac{Fl_{04}^3}{24EI_{04}} + \frac{t^2Fl_{02}^2}{12h^2EI_{04}} \left(l_{012} + \frac{l_{02}}{2}\right)$$
(17)

$$\theta_{03}(F, l_{0b}, l_{012}, l_{0b}, E) = \frac{Fl_{0b}}{2El_{0b}} (l_{0b} + 2l_{012})$$
 (18)

$$\delta_{03}(F, l_{0b}, I_{012}, I_{0b}, E) = \frac{F l_{0b}^2}{E I_{0b}} \left( \frac{l_{0b}}{3} + \frac{l_{012}}{2} \right)$$
 (19)

The angle and deflection of the DSU closest to the stressed end have been obtained in Section 3.1. For the second DSU, the angles and deflections of each segment can be computed one by one as below.

$$\begin{cases} \theta_{21} = \theta_{03}(F, L_{21}, L_1, I_{13}, E_2) \\ \delta_{21} = \delta_{03}(F, L_{21}, L_1, I_{13}, E_2) \\ \delta_{21} = \delta_{03}(F, L_{21}, L_1, I_{13}, E_2) \\ \delta_{24} = \delta_{03}(F, I_{24}, L_1 + I_{21}, I_{24}, I_{2}, h, E_2) \\ \theta_{2b} = \theta_{03}(F, I_{2b}, L_1 + I_{21} + I_{24}, I_{2b}, E_2) \\ \delta_{2b} = \delta_{03}(F, I_{2b}, L_1 + I_{21} + I_{24}, I_{2b}, E_2) \\ \theta_{25} = \theta_{02}(F, L_1 + I_{21} + I_{24} + I_{2b}, I_{25}, I_{25}, I_{2}, h, E_2) \\ \delta_{25} = \delta_{02}(F, I_{25}, I_1 + I_{21} + I_{24} + I_{2b}, I_{25}, I_{25}, I_{2}, h, E_2) \\ \theta_{23} = \theta_{03}(F, I_{23}, I_1 + I_{21} + I_{22}, I_{23}, E_2) \\ \delta_{23} = \delta_{03}(F, I_{23}, I_1 + I_{21} + I_{22}, I_{23}, E_2) \end{cases}$$

The deflection  $\delta_B$  of the second DSU can be obtained by substituting the parameters in Eq. (20) into Eq. (16 - 19) and then superimposing the results together.

$$\begin{split} \delta_{B} &= \delta_{21} + \delta_{2b} + \delta_{23} + \delta_{24} + \delta_{25} + \theta_{21}L_{1} \\ &+ \theta_{24}(L_{1} + l_{21}) + \theta_{2b}(L_{1} + l_{21} + l_{24}) \\ &+ \theta_{25}(L_{1} + l_{21} + l_{24} + l_{2b}) + \theta_{23}(L_{1} + l_{21} + l_{22}) \end{split} \tag{21}$$

Applying the same method for the third link, the deflection angle and deflection of each segment in the third DSU in Tri-DSU and the total deflection  $\delta_C$  of the third DSU can be obtained by Eq. (22-23).

$$\begin{cases} \theta_{31} = \theta_{03}(F, L_{31}, L_1 + L_2, I_{31}, E_3) \\ \delta_{31} = \delta_{03}(F, L_{31}, L_1 + L_2, I_{31}, E_3) \\ \theta_{34} = \theta_{02}(F, L_1 + L_2 + l_{31}, l_{34}, I_{34}, t_3, h, E_3) \\ \delta_{34} = \delta_{03}(F, l_{34}, L_1 + L_2 + l_{31}, I_{34}, t_3, h, E_3) \\ \theta_{3b} = \theta_{03}(F, l_{3b}, L_1 + L_2 + l_{31} + l_{34}, I_{3b}, E_3) \\ \delta_{3b} = \delta_{03}(F, l_{3b}, L_1 + L_2 + l_{31} + l_{34}, I_{3b}, E_3) \\ \theta_{35} = \theta_{02}(F, L_1 + L_2 + l_{31} + l_{32} - l_{35}, l_{35}, t_3, h, E_3) \\ \delta_{35} = \delta_{02}(F, l_{35}, L_1 + L_2 + l_{31} + l_{32} - l_{35}, I_{35}, t_3, h, E_3) \\ \theta_{33} = \theta_{03}(F, l_{23}, L_1 + L_2 + l_{31} + l_{32}, I_{33}, E_3) \\ \delta_{33} = \delta_{03}(F, l_{23}, L_1 + L_2 + l_{31} + l_{32}, I_{33}, E_3) \end{cases}$$

$$\begin{split} \delta_{C} &= \delta_{31} + \delta_{3b} + \delta_{33} + \delta_{34} + \delta_{35} + \theta_{31}(L_{1} + L_{2}) \\ &+ \theta_{34}(L_{1} + L_{2} + l_{31}) + \theta_{3b}(L_{1} + L_{2} + l_{31} + l_{34}) \\ &+ \theta_{35}(L_{1} + L_{2} + l_{31} + l_{34} + l_{3b}) \\ &+ \theta_{33}(L_{1} + L_{2} + l_{31} + l_{32}) \end{split} \tag{23}$$

Therefore, the total deflection  $\delta_{\text{total}}$  that acts on the end of the Tri-DSU can be calculated by accumulating the deflection of all three DSUs using Eq. (24).

$$\delta_{total} = \delta_A + \delta_B + \delta_C \tag{24}$$

# 4. FEA SIMULATION AND EXPERIMENTAL VALIDATION

# 4.1 Construction of the prototype

Based on the design and concept in Section 2, a Tri-DSU prototype was constructed by 3-D printing. PLA was chosen as the primary material due to its high toughness and strength characteristics. The design of the Tri-DSU was simplified during

the construction of the prototype. The three DSUs were printed directly as a single body. Linear actuators were not used, but rather the on and off of the solid blocks were implemented manually. When 3-D printing was performed, the prototype was filled with 40% and the layer height was 0.2mm.

# 4.2 Determination of material properties

The mechanical properties of the same material with various printing parameters are different. The properties of PLA are not provided at 40% filament, such as density, Young's modulus (E), and Poisson's ratio. Young's modulus was measured accordingly to its definition, i.e., the longitudinal stress divided by the strain. However, the results obtained were significantly smaller than the theoretical values. One reason could be that the 3-D printed parts are anisotropic due to the different patterns and fills at the time of printing. Thus resulting, the deflection equation for the cantilever beam was used as Eq. (3), which could best match the test scenario. Then we measured the force and deflection to calculate E which is 3472 MPa. To make the results as accurate as possible, a cantilever beam with similar dimensions to one DSU was used with the same print configuration of the whole Tri-DSU, being  $10 \times 20 \times 1$  mm. Moreover, we measured the density of PLA at 40% filling and 0.2 mm profiles to be 0.78 g/cm<sup>3</sup>. Also, the Poisson's ratio was determined to be 0.35, according to the negative of the ratio of transverse strain to axial strain.

### 4.3 FEA Simulation

In order to verify the accuracy of the analytical model in Section 3 and to find the optimal parameters of the DSU, we control the variables and define the width of the beam b, the length of the parallel beam segment  $l_2$ , and its thickness t as the independent variables in off mode, and in addition, for on mode, the scaling factor  $\lambda$  of the length of the  $l_4$  segment and the length of the solid block  $l_b$  are also considered. For each independent variable, ten models with different parameters were set. FEA simulations were performed on these models to analyze the static forces for various force scenarios. In ANSYS, a new PLA material was created by using the parameters measured in Section 4.2. The simulation was also performed for eight configurations of Tri-DSU, as described in Section 2. The parameters of the 3-D model used in the simulation are the same as those of the prototype used for the experiments. One end of the beam is fixed, and the other end is stressed and parallel to the Y-axis, which is similar to the force condition of a robotic arm in practical application.

# 4.4 Experimental Validation

To verify the accuracy of the FEA simulation, experiments on DSUs and Tri-DSUs were performed. As shown in Fig.5, a simplified 3-D printed Tri-DSU was mounted on a bench vise. The Mark-10 M5-100 force gauge was mounted on the ESM303 test stand to measure the force applied to the end of the beam. The flat tip shape of the probe was selected because it is the closest to the real load situation. The probe is placed at the end of the DSU, the force and displacement are zeroed, and the force

threshold is set. The probe will automatically depress until the threshold is reached, which is the same as the setting in ANAYS. To reduce the error, the experiment is repeated five times for each model and the results are finally averaged.

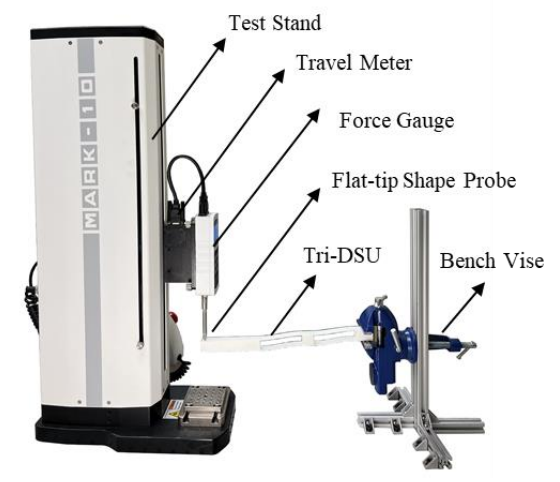
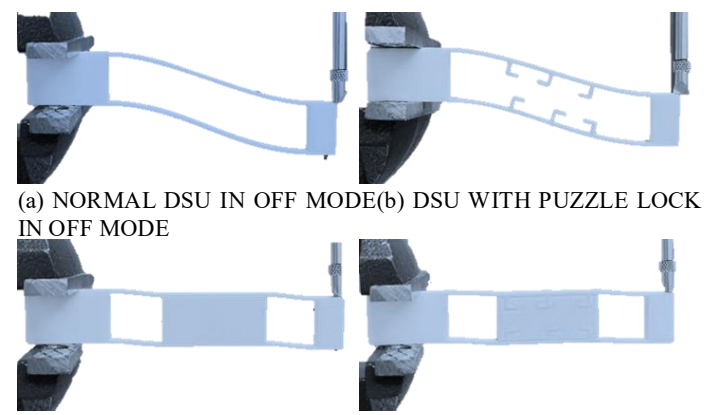


**FIGURE 5:** EXPERIMENTAL SETUP

### 4.5 Puzzle lock mechanism

As shown in Fig. 6, we designed the puzzle lock mechanism for the DSU to limit the unexpected sliding of the solid block in on mode in both x-axis and y-axis. the L-shape beam of the puzzle lock is only 1 mm thick to reduce the effect on the parallel beam deformation as much as possible. As shown in Fig. 6(a) and (b), in off mode, the stiffness of the DSU without puzzle lock is 0.065 N/mm, while the stiffness with puzzle lock is 0.066 N/mm. This indicates that in off mode, the puzzle lock has almost no effect on the deformation of the parallel beam. As shown in Fig. 6(c) and (d), in on mode, the stiffness of the conjoined DSU is 1.32 N/mm in the case of integrated printing frame and block, while the stiffness with puzzle lock is 1.24 N/mm, and the two stiffnesses are very close. However, as shown in Fig. 6(e), if the solid block inserted into the cavity is not restricted, it will significantly reduce the effect of variable stiffness, which is only 0.080 N/mm. This represents that the puzzle lock design can significantly solve the sliding problem of the solid block.



(c) CONJOINED DSU IN ON MODE(d) DSU WITH PUZZLE LOCK IN ON MODE



(e) NORMAL DSU (WITHOUT PUZZLE LOCK) IN ON MODE **FIGURE 6:** COMPARISON OF DSU WITH AND WITHOUT PUZZLE LOCK DESIGN

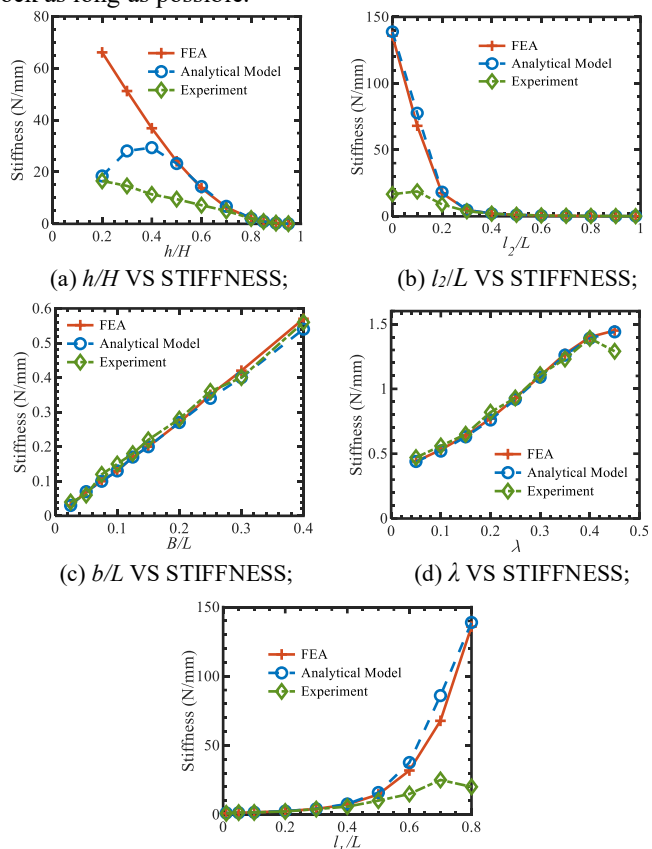
#### 5. RESULTS

## 5.1 Result analysis of the DSU

The deflection and stiffness data of DSUs with different parameters and configurations under various forces were collected by ANSYS simulations, MATLAB calculations, and experiments. To facilitate the analysis and comparison, we standardized the available parameters, for example, using h/H to denote the thickness ratio of the leaf spring. A larger value of this ratio means that the thickness of the leaf spring is smaller, which will theoretically reduce the stiffness of the whole DSU. The  $l_2/L$ represents the ratio of the length of the parallel beam. A larger value of  $l_2/L$  means a larger percentage of the compliant segment's length, which will also lead to a reduction in stiffness. b/L represents the width ratio of the DSU. A larger b/L means that the beam is wider and will increase its stiffness.  $\lambda$  reflects the change in the position of the solid block in the cavity. When  $\lambda$  tends to 0.5, this represents that the block is near the middle of the cavity and therefore the beam can obtain more stiffness. If  $\lambda$ tends to 0, it means that the block is near the end of the cavity and therefore the beam can obtain lower stiffness.  $l_b/L$  represents the percentage of the block for the whole beam length, which reflects the variation of the block size in the central region of the cavity. When the value of  $l_b/L$  rises, the stiffness of the DSU will increase. When  $l_b/L$  is 0, it represents that there is no solid block in the cavity in the off mode. When  $l_b/L = 1$ , this means that the DSU becomes a solid cantilever beam. The standard DSU mentioned in Section 2 is used in the experiment and FEA, where the parameters are kept constant when studying a single variable, except itself varied.

Fig. 7(a) illustrates the relationship between h/H value and stiffness, where the stiffness decreases when h/H increases. Obviously, when h/H is less than 0.4, the error between the theoretical value and FEA becomes large. One possible reason is that the analytical model overestimates the deformation of the parallel beam at the compliant segment. However, when h/H is greater than 0.4, which is in the normal design range, the model is still feasible. When h/H is less than 0.6, the error between the experimental value and FEA also becomes large. The most likely reason is that when the beam is thick, the deformation of the entire DSU is less than 1mm, and the error in percentage measurement will be magnified. When h/H is greater than 0.6, the error of all three values is less than 10%. Fig. 7(b) illustrates the relationship between b/L and stiffness, when its value increases, the stiffness also increases. In these cases, the errors in all of the theoretical and experimental values and FEA are less

than 5%. As shown in Fig. 7(c), the stiffness decreases when  $l_2/L$ increases. When  $l_2/L$  is less than 0.2, the error between FEA and the experimental value increases significantly, most likely for the same reason as in the case of h/H, while the error relative to the theoretical value and FEA is always within 5%. Fig. 7(d) shows the stiffness becomes larger with bigger  $\lambda$ . In these cases, the errors of all of FEA, theoretical and experimental values are less than 5% until  $\lambda = 0.5$ . As shown in Fig. 7(e), the stiffness increases when  $l_b/L$  increases, where the error between the FEA and the theoretical value is always less than 10%. However, when the value of  $l_b/L$  L is greater than 0.5, the error between the FEA and the experimental value increases significantly, most likely for the same reason as in the case of h/H. Therefore, to achieve a more significant change in stiffness, it is better to make the length of the parallel beam in the DSU as long as possible, the thickness of the leaf spring as thin as possible, and the solid block as long as possible.



(e) *l*<sub>b</sub>/*L* VS STIFFNESS. **FIGURE 7:** COMPARISON OF THE STIFFNESS OF THE DSU OF FEA, THEORETICAL VALUE, AND EXPERIMENTAL VALUE

## 5.2 Result analysis of the Tri-DSU

Fig. 8 shows the force and deflection relationships, i.e., stiffness relationships, of Tri-DSU under eight configurations. For each configuration, the error between the FEA and the theoretical values is less than 3%. For all seven configurations except the NNN mode, the errors between FEA and experimental values are less than 20%. For NNN mode, the error between FEA

and experimental values reaches 109%, which is because both of them have a deflection of less than 1 mm under the load of 2 N, so the error percentage is magnified. In fact, they have an error of only 0.4 mm. A better result could be achieved by using metallic materials without anisotropy such as aluminum or steel.

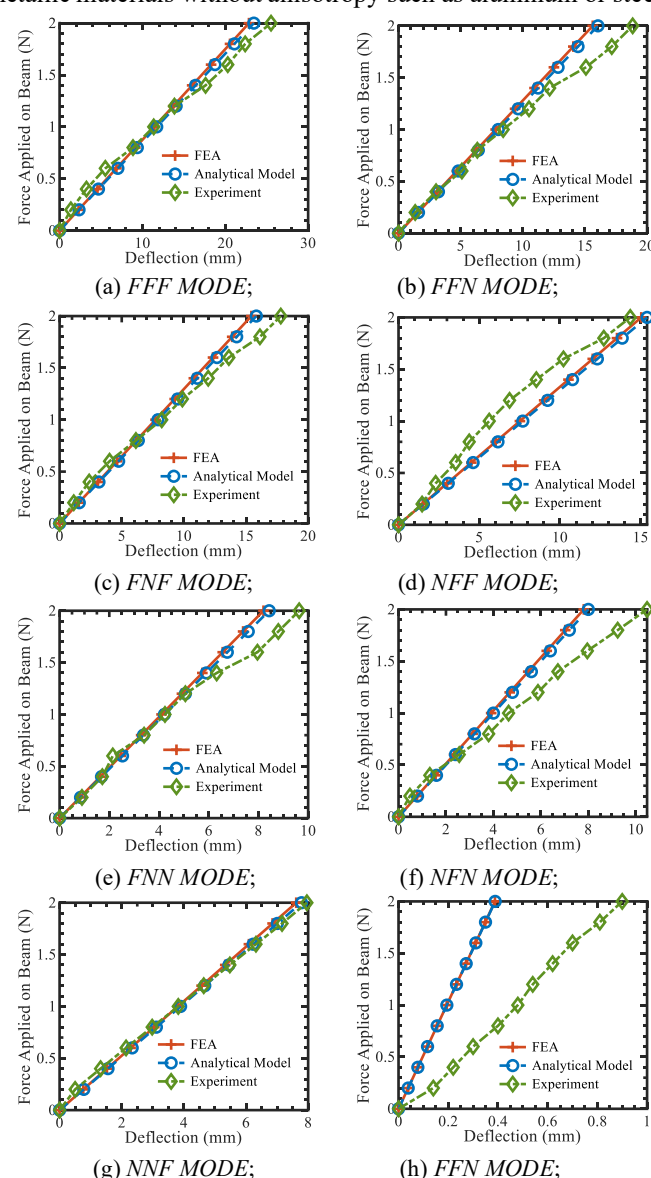


**FIGURE 8:** COMPARISON OF THE STIFFNESS OF THE TRI-DSU OF FEA, THEORETICAL VALUE, AND EXPERIMENTAL VALUE IN DIFFERENT CONFIGURATIONS

The minimum theoretical stiffness of Tri-DSU in the FFF mode is 0.09 N/mm, while the maximum theoretical stiffness in the NNN mode is 5.16 N/mm. Thus, Tri-DSU can theoretically achieve a 57-fold change in stiffness. Fig. 9 compares the experimental values of the eight configurations of Tri-DSU, which are consistent with the design in section 2. The FFN, FNF, and NFF modes have lower and similar stiffnesses, but different locations of the compliant segments. The FFN, NFN, and NNF modes have higher and similar stiffnesses, also different

locations of the compliant segments. The FFF mode has the lowest stiffness with an experimental value of 0.08 N/mm and the NNN mode has the highest stiffness with an experimental value of 2.47 N/mm. Therefore, the Tri-DSU can actually achieve a 31-fold variation in stiffness.

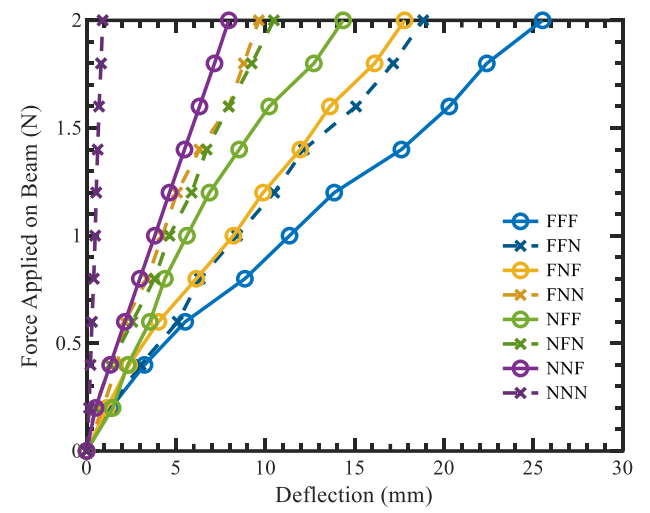


**FIGURE 9:** COMPARISON OF EXPERIMENTAL VALUE OF ALL MODES

#### 6. CONCLUSIONS

In this paper, a new concept of the discrete variable stiffness link is proposed for collaborative robots, leading to safe humanrobot interaction. The basic principle is to change the crosssectional area property of a hollow beam structure. The concept allows discrete variations of stiffness using linear actuators. The design features of Tri-DSU are elaborated including eight stiffness configurations. Based on the superposition principle, an analytical model for calculating the deflection and stiffness of the DSU segment by segment is established. It is also generalized to a mathematical model of Tri-DSU, which leads to modularity and customization and is also applicable to multiple DSU. Deflection and stiffness data of DSU with different parameters and configurations under various forces are collected through FEA simulations, mathematical analysis, and experiments. These data were compared and validated using the control variables method as well. The results were found to be feasible in most cases satisfying the expected accuracy which is 10%. However, the error of the analytical model will become larger at higher stiffnesses. The actual stiffness variation rate of Tri-DSU can reach 31 times, which is an innovative breakthrough. Next, we will apply the DSU concept to variable stiffness actuators and grippers.

## **ACKNOWLEDGMENT**

This work was funded by the National Science Foundation (NSF) grant under FRR-2131711 and the Purdue-Khalifa University collaboration project under award No. CIRA-2020-024.

### **REFERENCES**

[1] A.M. Djuric, J.L. Rickli, and R.J. Urbanic, A Framework for

- Collaborative Robot (CoBot) Integration in Advanced Manufacturing Systems, *SAE Int. J. Mater. Manuf.* 9 (2) (2016) 457–464.
- [2] I. Aaltonen, T. Salmi, and I. Marstio, Refining levels of collaboration to support the design and evaluation of human-robot interaction in the manufacturing industry, *Procedia CIRP* 72 (2018) 93–98
- [3] Y.J. Zhang et al., From Manual Operation to Collaborative Robot Assembly: An Integrated Model of Productivity and Ergonomic Performance, *IEEE Robot. Autom. Lett.* 6 (2) (2021) 895–902.
- [4] L. Rozo et al., Learning Physical Collaborative Robot Behaviors From Human Demonstrations, *IEEE Trans. Robot.* 32 (3) (2016) 513–527.
- [5] D. Gan et al., Stiffness design for a spatial three degrees of freedom serial compliant manipulator based on impact configuration decomposition, *J. Mech. Robot.* 5 (1) (2013) 11002-1-11002-10.
- [6] P. Ohta et al., Design of a Lightweight Soft Robotic Arm Using Pneumatic Artificial Muscles and Inflatable Sleeves, *Soft Robot.* 5 (2) (2018) 204–215.
- [7] H. Yang et al., Design and Implementation of a Soft Robotic Arm Driven by SMA Coils, *IEEE Trans. Ind. Electron.* 66 (8) (2019) 6108–6116.
- [8] X. Liang et al., Design, Characterization, and Implementation of a Two-DOF Fabric-Based Soft Robotic Arm, *IEEE Robot. Autom. Lett.* 3 (3) (2018) 2702–2709.
- [9] G. Tonietti, R. Schiavi, and A. Bicchi, Design and control of a variable stiffness actuator for safe and fast physical human/robot interaction, *Proc. IEEE Int. Conf. Robot. Autom.* 2005 (2005) 526–531.
- [10] L. Liu et al., Impedance-Controlled Variable Stiffness Actuator for Lower Limb Robot Applications, *IEEE Trans. Autom. Sci. Eng.* 17 (2) (2020) 991–1004.
- [11] R. Schiavi et al., VSA-II: A novel prototype of variable stiffness actuator for safe and performing robots interacting with humans, *in* Proc. IEEE Int. Conf. Robot. Autom., (2008): pp. 2171–2176.
- [12] Y. Zhu et al., Design and Evaluation of a Novel Torque-Controllable Variable Stiffness Actuator with Reconfigurability, *IEEE/ASME Trans. Mechatronics* (2021).
- [13] J. Choi et al., A robot joint with variable stiffness using leaf springs, *IEEE Trans. Robot.* 27 (2) (2011) 229–238.
- [14] Y. Xu et al., Design, modeling and control of a reconfigurable variable stiffness actuator, *Mech. Syst. Signal Process.* 160 (2021) 107883.
- [15] I. Hussain et al., Modeling, control, and numerical simulations of a Novel Binary-Controlled Variable Stiffness Actuator (BcVSA), *Front. Robot. AI* 5 (JUN) (2018) 68.
- [16] M.I. Awad et al., Design of a novel passive binary-controlled variable stiffness joint (BpVSJ) towards passive haptic interface application, *IEEE Access* 6 (2018) 63045–63057.
- [17] J. Shintake et al., Soft Robotic Grippers, *Adv. Mater.* 30 (29) (2018) 1707035.
- [18] L. Zhou et al., Bio-Inspired Soft Grippers Based on Impactive Gripping, *Adv. Sci.* 8 (9) (2021) 2002017.
- [19] T. Morrison and H.J. Su, Stiffness modeling of a variable stiffness compliant link, *Mech. Mach. Theory* 153 (2020) 104021.
- [20] T. Morrison et al., A novel rotating beam link for variable stiffness robotic arms, *Proc. IEEE Int. Conf. Robot. Autom.* 2019-May (2019) 9387–9393.
- [21] R. Hu, V. Venkiteswaran, and H.J. Su, A variable stiffness robotic arm using linearly actuated compliant parallel guided mechanism, *in* Mech. Mach. Sci., *Springer Netherlands*, (2019): pp. 33–40.

- [22] Y. She et al., Design, modeling, and manufacturing of a variable lateral stiffness arm via shape morphing mechanisms, *J. Mech. Robot.* 13 (3) (2021).
- [23] I. Hussain et al., Modeling, identification, and control of a discrete variable stiffness actuator (DVSA), *Actuators* 8 (3) (2019).
- [24] M.I. Awad et al., Passive discrete variable stiffness joint (PDVSJ-II): Modeling, design, characterization, and testing toward passive haptic interface, *J. Mech. Robot.* 11 (1) (2019).
- [25] J. Fu and D. Gan, A Reconfigurable Variable-Stiffness Parallel Beam for Compliant Robotic Mechanisms Towards Safe Human Interaction, *Proc. ASME Des. Eng. Tech. Conf.* 8A-2021 (2021).
- [26] Y. Luo, W. Liu, and L. Wu, Analysis of the displacement of lumped compliant parallel-guiding mechanism considering parasitic rotation and deflection on the guiding plate and rigid beams, *Mech. Mach. Theory* 91 (2015) 50–68.
- [27] V.K. Venkiteswaran and H.J. Su, Extension Effects in Compliant Joints and Pseudo-Rigid-Body Models, *J. Mech. Des. Trans. ASME* 138 (9) (2016).
- [28] S. Awtar and E. Sevincer, Elastic Averaging in Flexure Mechanisms: A Muliti-Beam Parallelogram Flexure Case-Study, *in ASME International*, (2006): pp. 251–257.
- [29] S. Awtar, K. Shimotsu, and S. Sen, Elastic averaging in flexure mechanisms: A three-beam parallelogram flexure case study, *J. Mech. Robot.* 2 (4) (2010).
- [30] L.L. Howell, S.P. Magleby, and B.M. Olsen, *Handbook of Compliant Mechanisms*, Wiley, (2013).
- [31] S. Awtar, A.H. Slocum, and E. Sevincer, Characteristics of beam-based flexure modules, *J. Mech. Des. Trans. ASME* 129 (6) (2007) 625–639.